

LAMINAR SEPARATION ON AN AIRFOIL WITH PERTURBATION OF OUTER AND INNER BOUNDARY CONDITIONS

Eike Tangermann[1], Anuhya Jagadeesha[1] & Markus Klein[1]

[1]Universität der Bundeswehr München, 85577 Neubiberg, Germany

Abstract

The process of laminar separation is very sensitive to perturbations of the outer and inner boundary conditions such as surface unevenness or ambient turbulence. This often makes it hard to compare results, where the boundaries are not fully congruent or not even fully characterized, which in particular often is the case between results from experiment and simulation. By means of numerical simulations, the present study provides an assessment of the impact of boundary perturbations to laminar separation on a quasi two-dimensional airfoil configuration. The two aspects of surface unevenness and ambient turbulence are considered in parametric variations and compared to the ideal baseline case in order to quantify the impact to the flow field.

Keywords: Laminar Separation, LES, Uncertainty

1. Background and Motivation

Flow over wings at moderately low Reynolds numbers ($Re \approx 10^4 \ldots 10^5$) as it appears in small (unmanned) aerial vehicles features specific fluid mechanic phenomena which have severe impact on the aerodynamic behavior. The flow, which initially remains laminar, tends to separate easily and then undergoes transition in the separated shear layer. The enhanced mixing in the turbulent flow transports streamwise momentum towards the wall and the flow can reattach as long as the angle of attack remains low enough. Hence, the laminar separation does not necessarily lead to wing stall with severe loss of lift but can extend the range of usable angles of attack. Nevertheless, it affects the aerodynamic behavior and performance of the wing. Its occurrence and development needs to be understood well in the design process.

The laminar boundary layers appearing here exhibit pronounced sensitivity to environmental disturbances, including freestream turbulence, surface roughness, and further imperfections. These factors introduce uncertainties that complicate direct comparisons between experimental measurements and numerical simulations. Experimental setups inherently contain residual freestream turbulence, minimal surface irregularities, and confinement effects, which are often unquantified. Conversely, simulations typically assume idealized conditions such as smooth walls, undisturbed inflow, and simplified outer boundary conditions. This discrepancy can lead to significant deviations in predicted separation locations, transition behavior, and aerodynamic forces, thereby undermining the reliability of computational fluid dynamics (CFD) for low-Reynolds-number applications.

Several studies addressing this topic can be found in the literature. Schmidt and Breuer [1] compare results featuring the SD7003 airfoil in different wind tunnels, concluding that background turbulence of the facilities is accountable for differences in the results. They then propose a method to account for ambient turbulence in scale-resolving CFD simulations. Typically, elevated background turbulence leads to perturbations of the laminar boundary layer, delays flow separation and accelerates transition. Based on their method, an advancement has been proposed by Tangermann and Klein [2] which is employed here.

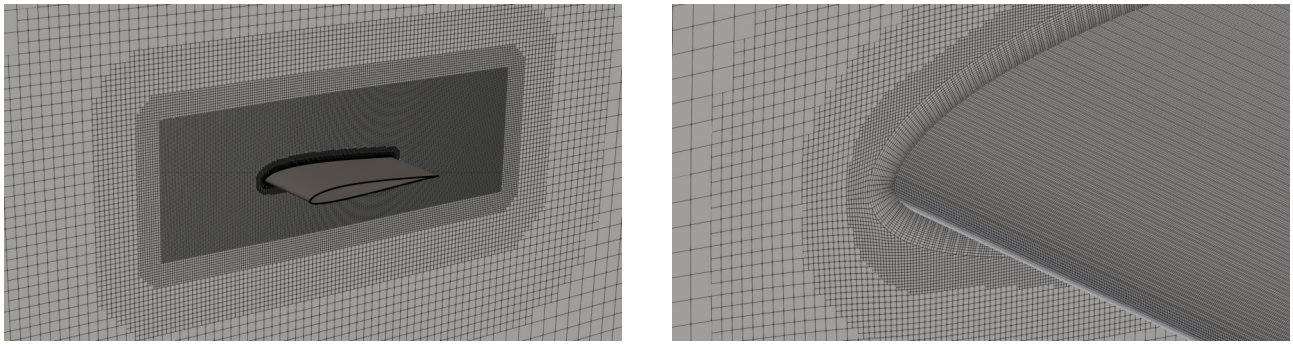


Figure 1 – Computational mesh for the simulations.

The effect of surface deviations has been demonstrated as well. Based on the setup of the experiments by Dierl et al. [3], from which the exact geometry of the wing has been measured, Tangermann et al. [4] have performed numerical simulations. Compared to an idealized smooth wing, which is typical for numerical simulations, the effect is in some aspects comparable to that of freestream turbulence. The laminar separation does not occur in a straight front any more but becomes wrinkled and fluctuates up- and downstream in time. The same holds for the Kelvin-Helmholtz vortices rolling up in the shear layer above the separation bubble. Unlike in idealized conditions, where they appear in straight lines [5], their formation and breakdown locations fluctuate. The resulting turbulent boundary layer shows no harmonic behavior. Even surface roughness of very low height ($y^+ < 0.5$) has the potential to induce perturbations to the laminar boundary layer.
The present study systematically investigates the influence of freestream turbulence and surface perturbations on laminar separation bubbles (LSBs) using large-eddy simulations (LES) of an SD7003 airfoil at $Re = 6 \cdot 10^4$. The underlying simulation methods have been established in previous work [4, 6, 7], where the background is discussed in more detail as well. In contrast to previous studies, which often use greater perturbations to study their effect, this work focuses on a minimal amount of perturbation. The objective is to establish a numerical framework of controlled conditions that demonstrates how these disturbances affect separation dynamics, transition mechanisms, and aerodynamic performance, thereby enhancing the predictive capabilities of CFD in general and in particular consistency between experimental and computational results.

2. Simulation Methodology

The flow field simulations employ the OpenFOAM Flow Solver [8] version 2412 featuring an incompressible formulation of the Navier-Stokes equations with finite volume numerical discretization. The accuracy of the numerical approach is of second order both in space and in time. The convective term is treated with linear interpolation. Temporal advancement is handled with an implicit backward scheme. Coupling of pressure and velocity in the incompressible context is achieved with the PISO method and iterative time advancement.
In order to capture and observe perturbation effects, it is required to resolve turbulent scales at least partially. The grid is relatively fine to cover small imperfections, whereas the turbulent structures at the moderate Reynolds number are comparably large. Hence, most turbulence is already resolved. The small amount of subgrid scales is considered using an LES model, namely the Wall-Adapting Local Eddy-Viscosity (WALE) model according to [9]. The WALE model exhibits the correct near-wall asymptotic behavior for wall-bounded flows, which is essential in the present application. This setup allows to resolve all relevant parts of the transitional flow while maintaining the computational effort reasonable.
The numerical mesh has an unstructured topology, based on hierarchical refinement of hexahedra towards the surface. Hanging nodes are avoided by insertion of polyhedra between the stages of cell refinement. Along the wing surface, cell layers ensure proper coverage of the gradients within the viscous sublayer. The non-dimensional thickness y^+ of the first cell on the wall in boundary layer coordinates is well below unity, cell widths then increase with a ratio of 1.07 to allow for a good resolution of the gradients. In stream- and spanwise direction the cells have approximately a size of

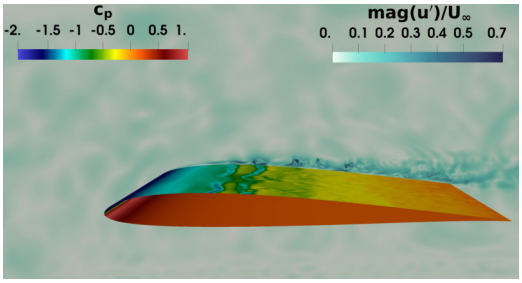
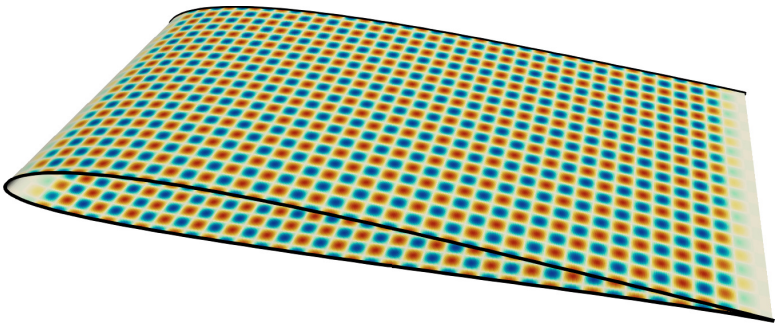
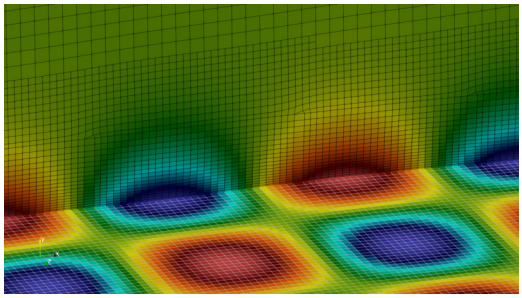


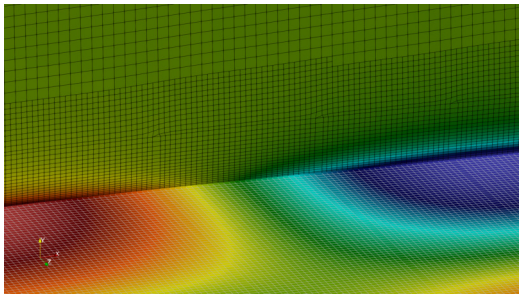
Figure 2 – Indication of instantaneous velocity fluctuations (u') around the wing in ambient turbulence with pressure coefficient (c_p) contours on the surface.

$x^+, y^+ \approx 3.37$ in non-dimensional boundary layer coordinates, which also is considered fine enough to capture all relevant physics of boundary layer turbulence in the context of LES. The model extends 0.5 times the chord length c in spanwise direction, which is sufficient to avoid interference from the cyclic boundary condition. A refinement box is located around the wing extending well upstream to account for the transport of ambient turbulence introduced slightly upstream of the wing. Figure 1 shows details of the turbulence box and the boundary layer mesh. With the farfield boundary located $20c$ away from the wing, the mesh results in a total of $39.5 \cdot 10^6$ cells. Before considering the perturbations, cases with ideally clean boundary conditions have been simulated to serve as a baseline.
Two primary uncertainty factors are examined. The first is freestream turbulence, which is introduced via volumetric forcing to prescribe turbulent kinetic energy (TKE) and length scales independently of the mean flow profile. In a case like here, it is unfeasible to introduce turbulence at the farfield boundary on top of the mean flow velocity. The fluctuations are rather introduced slightly upstream of the wing. Following the method described in [2], synthetically generated fluctuations are superimposed by local volume forces within a specified box. The fluctuations are generated from a random field filtered to the desired length scale and then scaled to the desired Reynolds stresses [10]. To ensure maintaining the correct intensity, a digital controller algorithm adapts their magnitude. Thus, length scale and intensity of the ambient turbulence can be prescribed independently in the parametric variation. Figure 2 provides a visualization of the resulting fluctuating field around the wing.
The second aspect considered is surface roughness. It is implemented explicitly resolved through





$\lambda = 0.05 \cdot c$



$\lambda = 0.2 \cdot c$

Figure 3 – Pattern of surface roughness with blue and red indicating deformation towards inside and outside, respectively. Deformation fades out towards leading and trailing edges.

Table 1 – Overview of investigated cases.

α	Turbulence	Surface
4°	–	–
4°	–	$h^+ = 1, \lambda = 0.05c$
4°	–	$h^+ = 2, \lambda = 0.2c$
4°	–	$h^+ = 4, \lambda = 0.2c$
6°	–	–
6°	$Tu = 1.2\%, \ell_t = 0.14c$	–
6°	$Tu = 1.7\%, \ell_t = 0.14c$	–

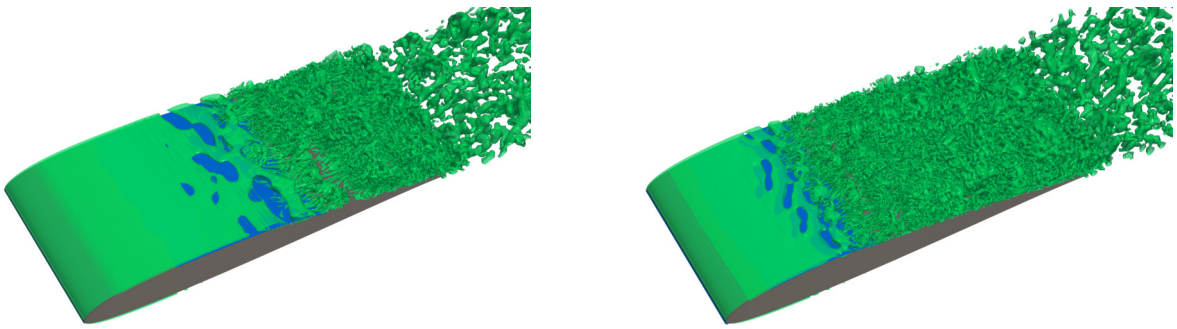
geometric deformation of the airfoil surface and the adjacent mesh cells with regular patterns of in- and outward pointing bumps. The bumps follow a positive and negative wall-normal displacement prescribed by the function $\cos(x \cdot 2\pi/\lambda) \cdot \cos(z \cdot 2\pi/\lambda)$ scaled with the intended height, where x and z denote chordwise and spanwise directions, respectively. The wave length λ determines the size of the structures. Using laplacian smoothing, the surface displacement is propagated into the flow domain. Figure 3 shows the surface pattern and its development into the flow field.

3. Results and Discussion

In the following sections results from the different cases will be presented. For a general overview to the underlying processes in the flow field, first a brief overview of the clean baseline case will be given. Then the effect of ambient turbulence is discussed followed by that of surface roughness. For a brief overview the investigated cases are summarized in Table 1.

3.1 Baseline Flow Field

Two angles of attack (α) have been considered. At $\alpha = 4^\circ$ the laminar boundary layer remains attached until passing 20% chord length, enters transition around 50% and reattaches between 60% and 70%. A slight increase to $\alpha = 6^\circ$ shifts the process significantly upstream. The separation already takes place at 10% chord length. Consequently the transition starts at 30% and after passing 40% the flow is nearly completely reattached. Thereby the flow at lower angles of attack is more susceptible to surface imperfections as the attached laminar boundary layer extends over a longer distance.
An instantaneous view to the flow is given by Figure 4. It shows an isosurface from Q criterion (green) above the separated region (blue). The offset of all processes between the two angles of attack becomes obvious. After passing the separation, the Q surface breaks up by Kelvin-Helmholtz (K-H) vortices above the separation bubble. With the breakup of the K-H vortices an attached turbulent boundary layer quickly forms. In particular at 4° gaps in the turbulent flow appear initially which result from the spacing between the K-H vortices. As the turbulence develops further, these gaps are filled but in fact pressure minima as traces from the K-H vortices remain embedded in the turbulent flow



$\alpha = 4^\circ$ $\alpha = 6^\circ$

Figure 4 – Instantaneous flow field indicated by an isosurface of the Q criterion (green). Separated flow is marked by the blue surface.

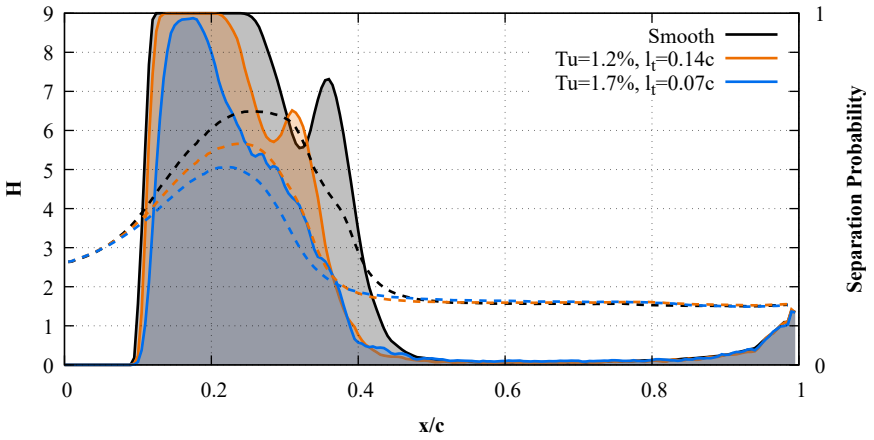


Figure 5 – Comparison of clean and turbulent freestream cases in terms of separation probability (solid lines) and boundary layer shape factor H (dashed lines).

[5]. This phenomenon is clearly related with the idealized simulation conditions. Already at slight perturbations the formation and breakup of the K-H vortices takes place far more irregular.

3.2 Influence of Freestream Turbulence

In the context of ambient turbulence, the simulations feature an angle of attack of $\alpha = 6°$. Inspired by the description of the experimental setup in a water towing tank from Reference [3], the fluctuation properties of the first case are an intensity of $Tu = 1.2\%$ with a length scale of $\ell_t = 0.14c$, where c again denotes the airfoil chord length. The fluctuations in the water tank are residual from a preceding experiment, which still can be detected even after a certain relaxation time, but in wind tunnels comparable background turbulence is present as well. The low intensity of 1.2% is hardly visible in flow field visualizations but already has an effect. A second case with higher intensity and smaller scales has been considered as well, which features $Tu = 1.7\%$ and $\ell_t = 0.07c$, where the fluctuations easier impinge into the boundary layer.

Figure 5 provides a first impression of the changes by the turbulent flow. It shows the presence of separated flow together with the boundary layer shape factor H. In the clean and low intensity cases the separation occurs nearly identical with only slight streamwise variations and a steep increase of the separation probability. The higher intensity case starts to separate at the same location but then stronger variations lead to a slower increase of the separation probability. With a maximum below unity, the high intensity case does not even show full separation across the span. In both turbulent cases the transition takes place sooner as the breakdown of K-H vortices is accelerated by impinging fluctuations. The longer length scale shows a very similar reattachment behavior as the clean case but shifted upstream by nearly $10\%c$. The smaller length scales lead to a quicker breakup, which causes a different characteristic of the separation probability. The reattachment, however, is reached identically in both turbulent cases. The shape factor behaves accordingly and reaches lower maxima with stronger ambient turbulence and reduced separation.

With the delayed transition in the clean case, the separation bubble has more space to grow and hence reaches a greater thickness. This also affects the thickness of the boundary layer downstream. Figures 6 and 7 underline this. The 99% thickness δ_{99} shows this trend only slightly but in the plots of displacement thickness δ^* and momentum loss thickness Θ it is visible very clearly.

The transition process is characterized by an increase of not only fluctuation intensity but also Reynolds shear stress. Figure 8 shows their development in the different cases. The turbulence kinetic energy (TKE) starts to rise slightly very soon, which results from the growth of the K-H vortices and is not actual turbulence. Once they break down, the Reynolds shear stress $-\langle u'v' \rangle$ starts to rise. They reach a peak at the end of the separation bubble. The plot demonstrates that higher inflow turbulence reduces peak TKE and advances transition, reducing the size of the separated region. Post-reattachment, the turbulent boundary layer exhibits minimal sensitivity to inflow conditions, indicating dominance by local shear dynamics.

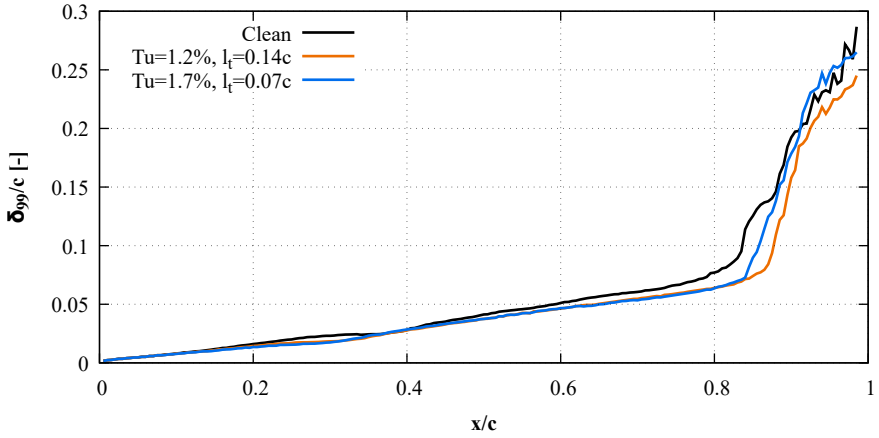


Figure 6 – 99% boundary layer thickness (δ_{99}) in clean and perturbed inflow conditions.

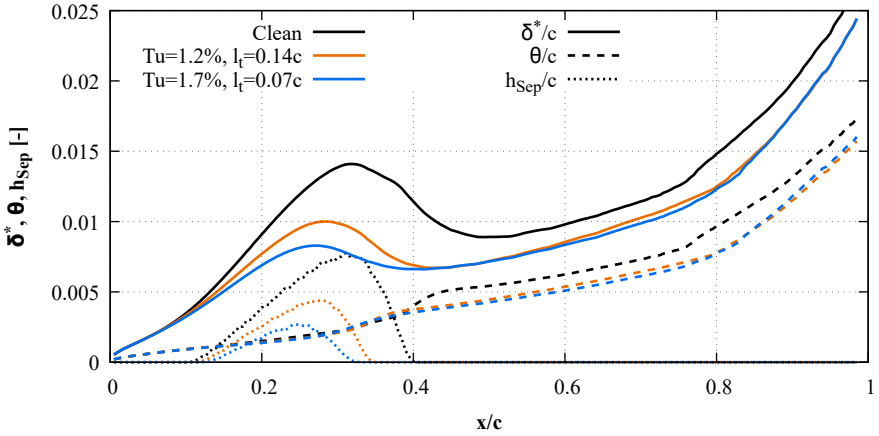


Figure 7 – Displacement (δ^*) and momentum loss thickness (Θ) together with separation bubble thickness (h_{Sep}).

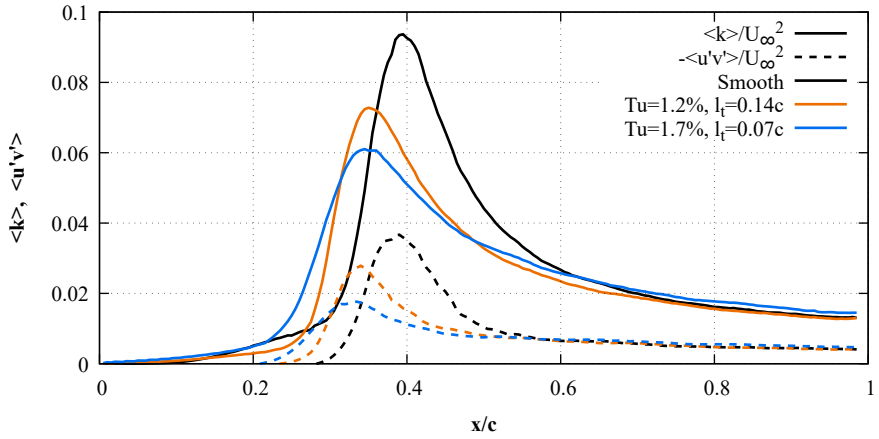


Figure 8 – Development of TKE k along the line of the boundary layer displacement thickness. Ambient turbulence gradually accelerates transition while reducing the peak TKE.

The smooth-wing baseline exhibits a well-defined LSB coming with a pronounced suction plateau. Besides the effects shown for flow field, the introduction of freestream turbulence also results in changes to global aerodynamics. The accelerated reattachment with reduction of the pressure plateau reduces lift. Pressure drag is reduced as well, whereas friction drag increases resulting in a lower overall glide efficiency.

3.3 Influence of Surface Roughness

Three roughness configurations were evaluated at an angle of attack of $\alpha = 4^\circ$ allowing for a longer development of perturbations along the rough wall. The first case has a roughness height in viscous wall units of $h^+ = 1$ and a wavelength of $\lambda = 0.05c$. The second and third case both feature $\lambda = 0.2c$ with roughness heights of $h^+ = 2$ and 4, respectively. The height might appear negligibly small, which is true for a turbulent boundary layer. In the laminar region, however, it already has a significant impact introducing perturbations which affect the following process.

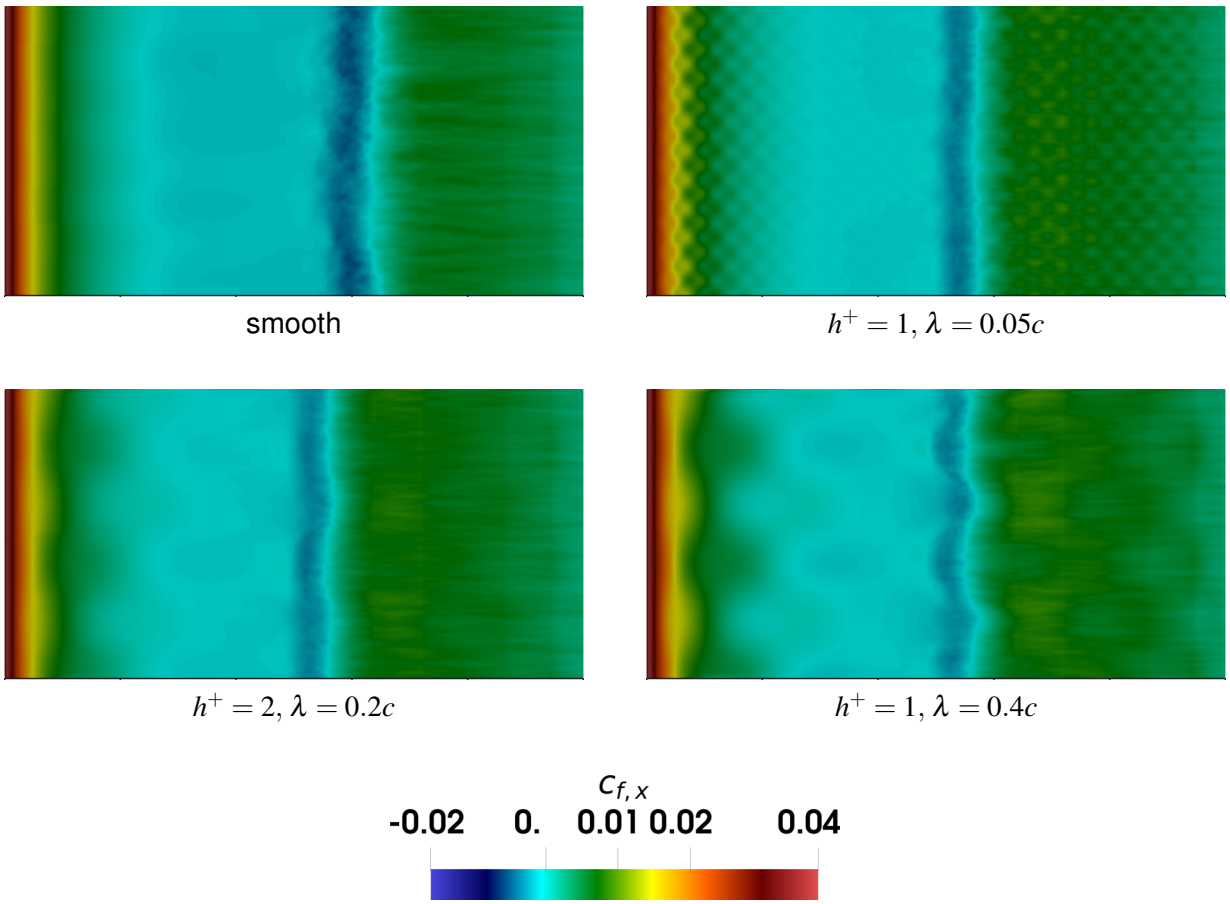


Figure 9 – Streamwise surface friction coefficient $\langle c_{f,x} \rangle$ along the wing surface. (Flow direction from left to right.)

The distribution of the roughness elements causes inhomogeneous profiles of the averaged flow properties in spanwise direction. This is underlined by the plots of temporally averaged surface friction in Figure 9. The smooth case is not perfectly homogeneous as well but when averaged in spanwise direction the solution statistics are fully converged. In the rough cases the inhomogeneity is significantly stronger. The footprint of the roughness elements is obvious. All values discussed below result from spanwise averaging of the flow field data and do not represent these variations.

On the rough wing, the separation behavior shown in Figure 10 changes in a way comparable to the case of low freestream turbulence. The higher the surface roughness amplitude, the wider is the range along which the separation front extends. The onset of the separation, however, hardly changes besides in the case of the highest roughness, where a small amount of earlier separation occurs. All three roughness cases show a very similar transition and reattachment process. The lines in Figure 10 nearly coincide and all show a reattachment approximately $10\%c$ sooner than on the smooth wing.

In terms of boundary layer thickness, the effect also is similar as seen in the freestream turbulence cases. The roughness shortens the LSB and thus leads to a thinner turbulent boundary layer. Between the different roughness cases only slight differences appear. Figure 11 shows the development of the boundary layer thickness measures. The curves from the rough cases are again very close,

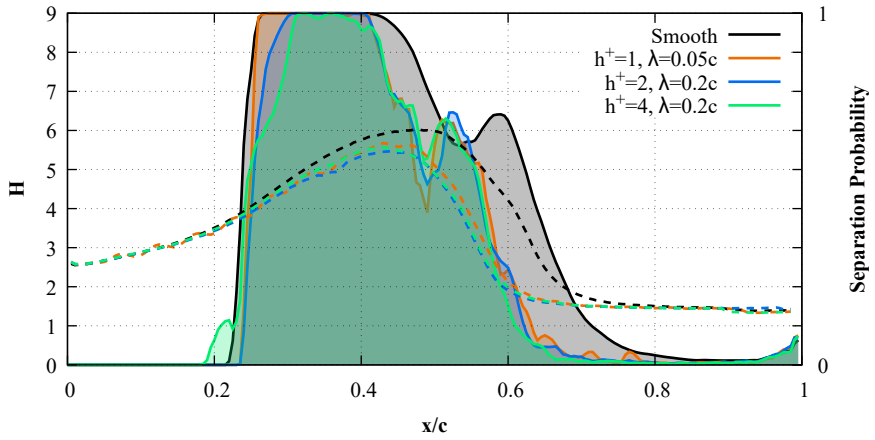


Figure 10 – Comparison of smooth and rough surface cases in terms of separation probability (solid lines) and boundary layer shape factor H (dashed lines).

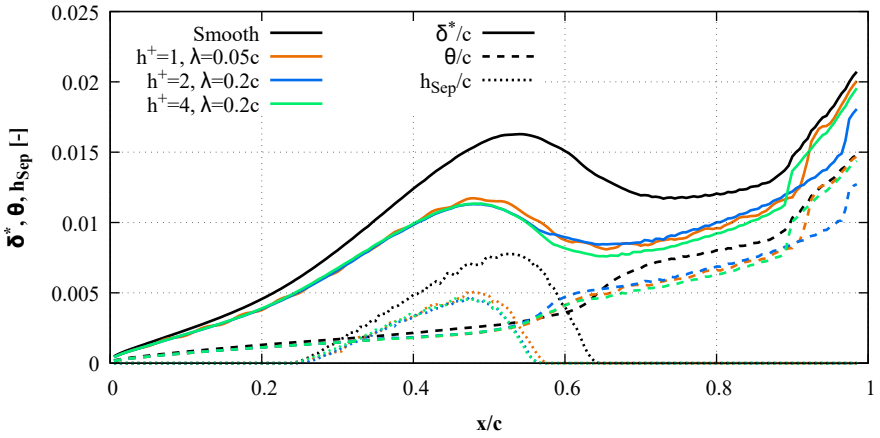


Figure 11 – Comparison of smooth and rough surface cases in terms of separation probability (solid lines) and boundary layer shape factor H (dashed lines).

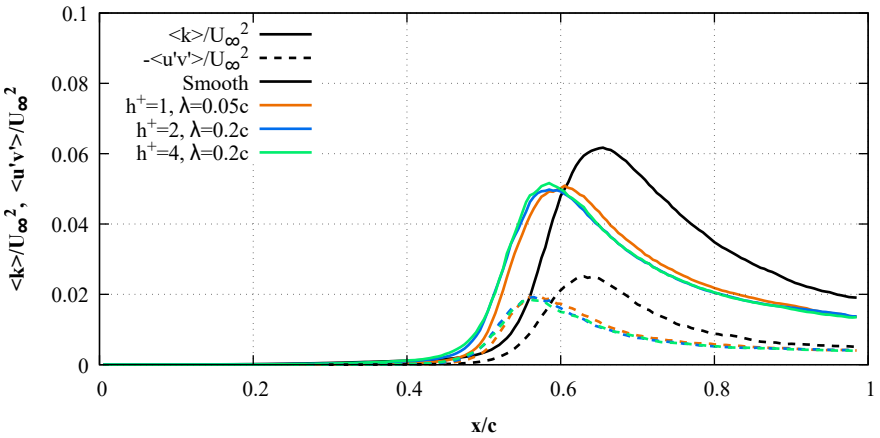


Figure 12 – Development of TKE k along the line of the boundary layer displacement thickness. Roughness has a similar effect as ambient turbulence but the present cases do not show a gradual variation.

which is in contrast to the effect of ambient turbulence, where a gradual change of the thickness appears with variation of the intensity.
In the development of turbulence during the transition the trend produced by the rough surface also

is similar to that seen from the freestream turbulence. The peak of TKE and Reynolds shear stress is not only shifting upstream, its magnitude is reduced, too. Figure 12 shows their development along the wing. Again the lines from all rough cases nearly coincide, indicating that on the one hand the selected parameter ranges do not cover the very onset of the effect, on the other hand the effect does not significantly scale within these roughness values.

4. Conclusions

Based on numerical simulation data, this study demonstrates that laminar separation is highly sensitive to freestream turbulence and surface roughness, with both factors capable of shortening the separation bubble, advancing transition, and modifying aerodynamic forces. In freestream turbulence the shortening of the LSB and all coupled effects increases gradually with fluctuation intensity. The trend can be seen clearly between the investigated cases.

Surface roughness has a similar effect. Even small roughness heights ($h^+ = 1 \ldots 4$) trigger earlier transition, compress the bubble and alter pressure recovery. The response, however, is very similar in all investigated cases, and the present study does not reveal a gradual scaling of the effect or the onset of the mechanism.

Post-reattachment, the turbulent boundary layer exhibits limited dependence on upstream disturbances, suggesting that its dynamics are governed by local shear rather than inflow history. These findings highlight the importance of accounting for uncertainties in low-Reynolds-number flows and provide valuable insights for improving consistency between experimental and numerical studies. Future work will extend the investigated parameter range to develop methods and formulations for quantifying the impact of such perturbations.

5. Copyright Statement

The authors confirm that they, and/or their company or organization, hold copyright on all of the original material included in this paper. The authors also confirm that they have obtained permission, from the copyright holder of any third party material included in this paper, to publish it as part of their paper. The authors confirm that they give permission, or have obtained permission from the copyright holder of this paper, for the publication and distribution of this paper as part of the ICAS proceedings or as individual off-prints from the proceedings.

References

[1] Stefan Schmidt and Michael Breuer. Source term based synthetic turbulence inflow generator for eddy-resolving predictions of an airfoil flow including a laminar separation bubble. *Computers & Fluids*, 146:1–22, 2017.

[2] Eike Tangermann and Markus Klein. Controlled synthetic freestream turbulence intensity introduced by a local volume force. *Fluids*, 5(3):130, August 2020.

[3] Wolfgang Dierl, Serhiy Yarusevych, Rainer Hain, and Christian J. Kähler. The formation process of a laminar separation bubble over an SD7003 airfoil at various accelerations. In Christian J. Kähler, Thomas Fuchs, Rainer Hain, Sven Scharnowski, Bodo Ruck, and Alfred Leder, editors, *30. Fachtagung Experimentelle Strömungsmechanik*, Karlsruhe, 2023. German Association for Laser Anemometry GALA e.V.

[4] Eike Tangermann, Wolfgang Dierl, and Markus Klein. Sensitivity of laminar separation to geometric uncertainties. In *AIAA SCITECH 2025 Forum*. American Institute of Aeronautics and Astronautics, January 2025.

[5] Eike Tangermann and Markus Klein. Coherent Flow Structures Downstream of a Laminar Separation Bubble – a Numerical Investigation. In *AIAA SCITECH 2024 Forum*, 2024.

[6] Eike Tangermann and Markus Klein. On hybrid RANS-LES of transition in a separated boundary layer. *International Journal of Heat and Fluid Flow*, 103:109188, October 2023.

[7] Eike Tangermann and Markus Klein. Numerical Simulation of a Separating Laminar Boundary Layer Exposed to Ambient Turbulence. In *14th WCCM-ECCOMAS Congress*. CIMNE, 2021.

[8] Hrvoje Jasak. *Error analysis and estimation for finite volume method with applications to fluid flow*. PhD thesis, Imperial College, London, 1996.

[9] Franck Nicoud and Frédéric Ducros. Subgrid-Scale Stress Modelling Based on the Square of the Velocity Gradient Tensor. *Flow, Turbulence and Combustion*, 62(3):183–200, 1999.

[10] Andreas Kempf, Markus Klein, and Johannes Janicka. Efficient generation of initial-and inflow-conditions for transient turbulent flows in arbitrary geometries. *Flow, Turbulence and combustion*, 74(1):67–84, 2005.